Chapter 1

Mie-Scattering Ellipsometry

Yasuaki Hayashi and Akio Sanpei

Additional information is available at the end of the chapter

http://dx.doi.org/10.5772/intechopen.70278

Abstract

The size and refractive index of particles can be analyzed through the measurement of polarization state of scattered light. The change of polarization state in Mie scattering has been represented by ellipsometric parameters, Ψ and Δ, like the reflection ellipsometry. The analysis method is called Mie-scattering ellipsometry. By in-process Mie-scattering ellipsometry, the growth processes of carbon particles in argon plasma and in methane plasma were analyzed. It was found that carbon particles grow by coagulation in argon plasma, while they grow by carbon coating in methane plasma. It is also shown that imaging Mie-scattering ellipsometry has the potential for the easier confirmation of optical adjustment from a long distance, as well as for the analysis of spatial distribution of particle size.

Keywords: Mie-scattering ellipsometry, Mie scattering, fine particles, monitoring, imaging ellipsometry, imaging Mie-scattering ellipsometry, dusty plasma, Coulomb crystal

1. Introduction

In the same way as in the commonly-used ellipsometry for thin-film analysis by the reflection of polarized light, the size and refractive index of particles can be analyzed through the measurement of polarization state of the scattered light. The change of polarization state in the size range of Mie scattering is able to be defined by using ellipsometric parameters, Ψ and Δ, like the reflection ellipsometry. The analysis method is called Mie-scattering ellipsometry [1–3].

The evaluation of size and size distribution of fine particles is important for their research and production. Since 1994, it has become possible to observe fine particles stationarily suspended in plasmas forming Coulomb crystals [3–5]. In such states, the position and movement of individual fine particles are easily analyzed.

Mie-scattering ellipsometry, including polarization-sensitive light scattering measurement method, was applied for the analyses of the growth of fine particles of amorphous carbon

[2, 3, 6–9] and amorphous silicon [10]. Lately, image sensors were used for the detection of scattered light instead of photodetector [11, 12]. It is a kind of imaging ellipsometry of Mie scattering. Imaging Mie-scattering ellipsometry has the potential for the analysis of spatial distribution of particle size and the easy confirmation of optical adjustment from a long distance [12].

Mie-scattering ellipsometry in Ψ-Δ two-dimensional (2D) plane enables more detailed analysis than the conventional polarization-ratio method [13] or polarization-sensitive method [9], which effectively applies only one ellipsometric parameter in the size region of monotone function. Although "scattering ellipsometry" was termed in the book of "Ellipsometry and Polarized Light" by Azzam and Bashara [14], the detailed description of its analytical method is not shown there. The analysis of trajectory of ellipsometric parameters depicted in the Ψ-Δ coordinate plane by *in situ* ellipsometry during growth of fine particles brings a lot of information about the growth in the same way as the *in situ* refection ellipsometry during film growth [15–21].

In this chapter, the principium of Mie-scattering ellipsometry, its application, imaging method, and their systems are presented.

2. Principium of Mie-scattering ellipsometry

In the same way as in the reflection ellipsometry, ellipsometric parameters Ψ and Δ for the Mie scattering are defined by the ratio between two complex scattering amplitudes in the direction parallel to the scattering plane and their vertical direction [1]. When particles are spherical and monodisperse, the ellipsometric parameters Ψ and Δ are defined by the ratio of the scattering amplitude functions [22] of a parallel polarization component ($\boldsymbol{S_p}$), which is in the scattering plane, to that of a perpendicular one ($\boldsymbol{S_s}$) as

$$\tan\Psi \cdot \exp(\mathrm{i}\Delta) = \frac{\boldsymbol{S_p}}{\boldsymbol{S_s}} \tag{1}$$

$\boldsymbol{S_p}$ and $\boldsymbol{S_s}$ are complex numbers and functions of the scattering angle, the diameter of particles, and the refractive index. The procedures of calculation of $\boldsymbol{S_p}$ and $\boldsymbol{S_s}$ from particle size and its optical index are given in [22, 23].

When particles are polydisperse in the size range of Mie scattering, the scattered light generally results in some depolarization even if the incident light is fully polarized [24]. In this case, the Stokes vector and the Mueller matrix are required for the calculation of polarization state. When incident light is linearly polarized with the azimuth at 45° to the scattering plane, the Stokes vector of scattered light from a particle "i" of a certain diameter is

$$\begin{pmatrix} I_i \\ Q_i \\ U_i \\ V_i \end{pmatrix} = I_0\left(|\boldsymbol{S_p}|^2 + |\boldsymbol{S_s}|^2\right)\begin{pmatrix} 1 \\ -\cos(2\Psi_i) \\ \sin(2\Psi_i)\cos(\Delta_i) \\ -\sin(2\Psi_i)\sin(\Delta_i) \end{pmatrix}, \tag{2}$$

where Ψ_i and Δ_i are the ellipsometric parameters for the particle " i," and I_0 is a constant proportional to the particle density and independent of the diameter. The total Stokes vector of polydisperse particles is obtained by the summation of all Stokes vectors as

$$I = \sum_i I_i, \qquad Q = \sum_i Q_i, \qquad U = \sum_i U_i, \qquad V = \sum_i V_i. \tag{3}$$

Generally, the two polarization components of the light scattered from polydisperse particles are imperfectly coherent. When the degree of coherence is expressed by μ, the ellipsometric parameters Ψ and Δ for the particles are defined here with the Stokes parameters as

$$\begin{pmatrix} I \\ Q \\ U \\ V \end{pmatrix} = I \begin{pmatrix} 1 \\ -\cos(2\Psi) \\ \mu \sin(2\Psi)\cos(\Delta) \\ -\mu \sin(2\Psi)\sin(\Delta) \end{pmatrix}, \tag{4}$$

that is,

$$\Psi = -\frac{1}{2}\cos^{-1}\frac{Q}{I}, \tag{5a}$$

$$\Delta = -\tan^{-1}\frac{V}{U} \quad \text{for } U \geqq 0, \quad \text{otherwise} \bigoplus 180^\circ. \tag{5b}$$

Thus, the ellipsometric parameters Ψ and Δ for polydisperse particles are obtained independently of the degree of coherence μ.

3. Monitoring and analyses by Mie-scattering ellipsometry

3.1. Ψ-Δ trajectory in growth of polydisperse fine particles

The ellipsometric parameters of polydisperse particles are calculated as functions of mean size and size distribution spread. For the calculation, the lognormal size distribution function, which was verified as appropriate to apply to the coagulation process of particles [25], is expressed as

$$N(D) = \frac{1}{\sqrt{2\pi}D\ln\sigma} e^{-\frac{(\ln D - \ln D_m)^2}{2(\ln\sigma)^2}}, \tag{6}$$

where D is the particle diameter, D_m is the geometric mean diameter, and σ is the geometric standard deviation.

Figure 1 shows the evolution of the ellipsometric parameters in the increase of geometric mean diameter with the refractive index of 2.5–0.75i, which is the value for an evaporated carbon foil, the scattering angle of 90°, and the geometric standard deviations of 1.0 (monodispersion), 1.2, and 1.5.

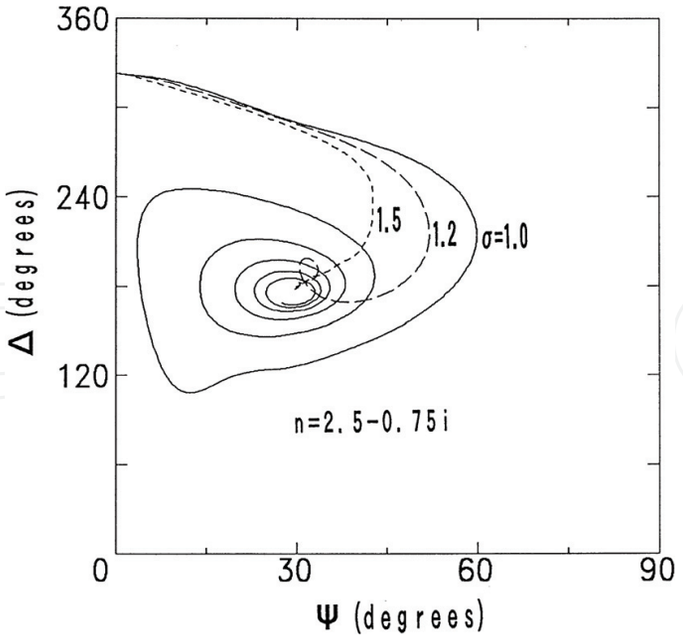

Figure 1. Calculated trajectories of the ellipsometric parameters for growing particles. Values used in the calculation are: 2.5–0.75*i* for the refractive index, 90° for the scattering angle, and 1.0, 1.2, and 1.5 for the geometric standard deviations [1].

3.2. System layout for Mie-scattering ellipsometry

Figure 2 shows the system layout for the Mie-scattering ellipsometry. The incidence light beam from an argon-ion laser (wavelength: 488 nm, output power: 100 mW) was linearly polarized at an azimuth of 45° from the plane of scattering through a Glan-Taylor prism polarizer. Its polarization state is expressed as $\chi = 1$, because $E_p = E_s$. After the scattering from particles in plasma, the polarization state of the light χ' was determined at a right angle from the incident beam line by use of a rotating-analyzer system directly driven by a stepper motor [26]. Light intensity was measured during the rotation of analyzer by two modes: with and without a quarter-wave plate, by using a computer-controlled in-and-out mechanism. When the fast axis of the quarter-wave plate is set in the scattering plane, scattered light intensity changes with analyzer azimuth A as

$$\mathcal{I}(A) = I + Q\cos 2A + U\sin 2A \quad \text{for without quarter-wave plate,} \tag{7a}$$

$$\mathcal{I}(A) = I + Q\cos 2A + V\sin 2A \quad \text{for with quarter-wave plate.} \tag{7b}$$

Thus, all four Stokes parameters are determined through the Fourier integral of Eqs. (7a) and (7b). Then, the ellipsometric parameters Ψ and Δ, which is uniquely determined in the full range of 360°, are calculated by Eqs. (5a) and (5b).

A parallel-plate rf (radio frequency) discharge reactor (rf electrode diameter: 5 cm, grounded electrode size: 22 cm × 6.5 cm, and separation of the electrodes: 2.0 cm) was used in the experiments (**Figure 3**). Argon or methane gas was introduced into the chamber at a position far from the plasma region so as not to disturb or evacuate the suspended particles with its flow. After the generation of plasma at a pressure of 40 Pa and an rf power of 2 or 8 W, the

http://dx.doi.org/10.5772/intechopen.70278

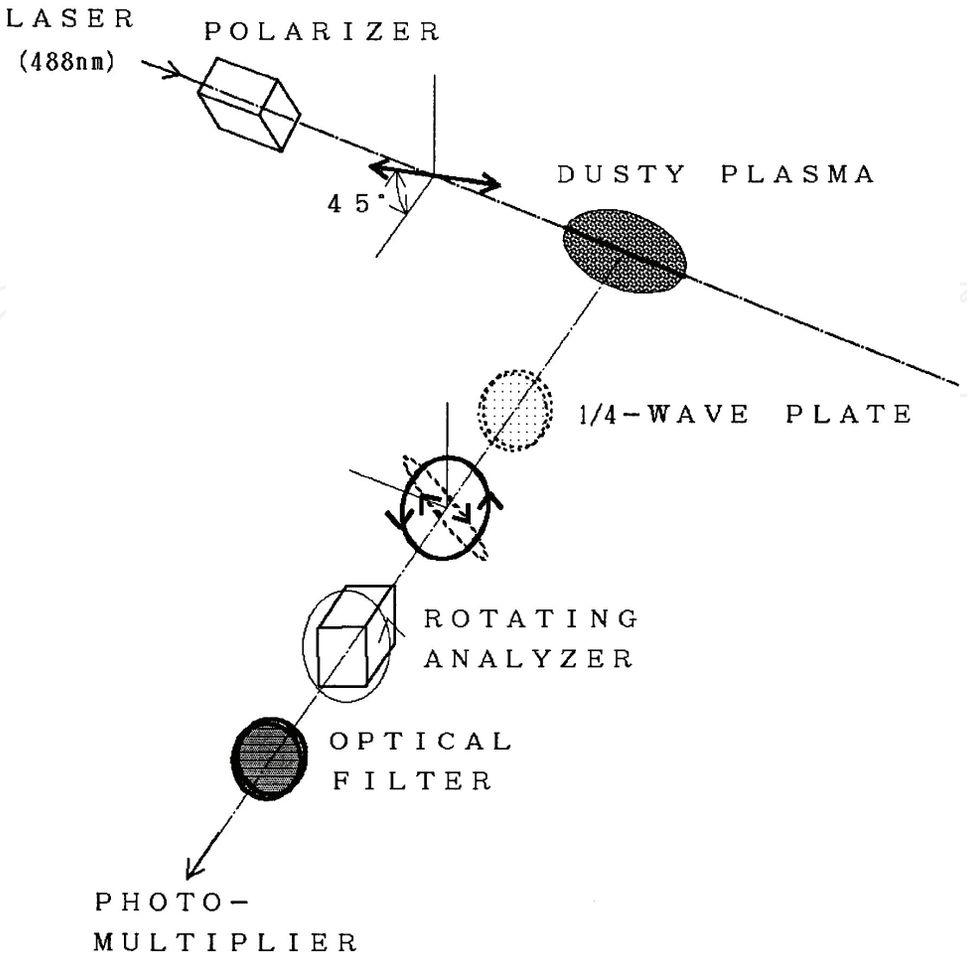

Figure 2. Schematic arrangement for the measurement of Mie-scattering ellipsometry. Incident light from an argon-ion laser is linearly polarized. The polarization state of light scattered from particles is analyzed with the use of a quarter-wave plate and a rotating-analyzer system [1].

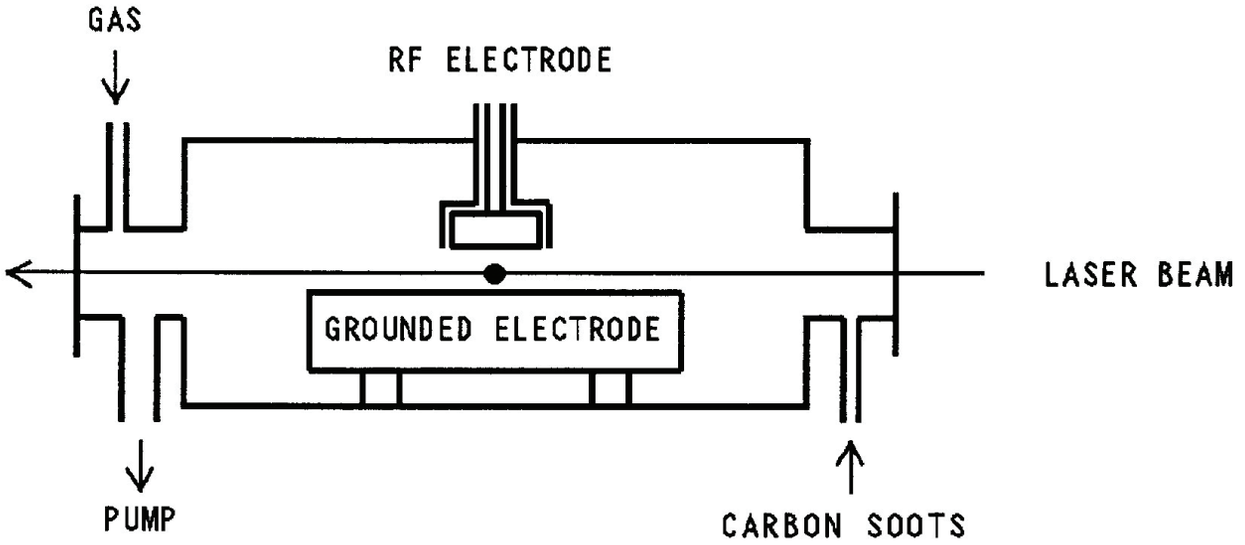

Figure 3. Experimental setup for the measurement of carbon particle growth [2].

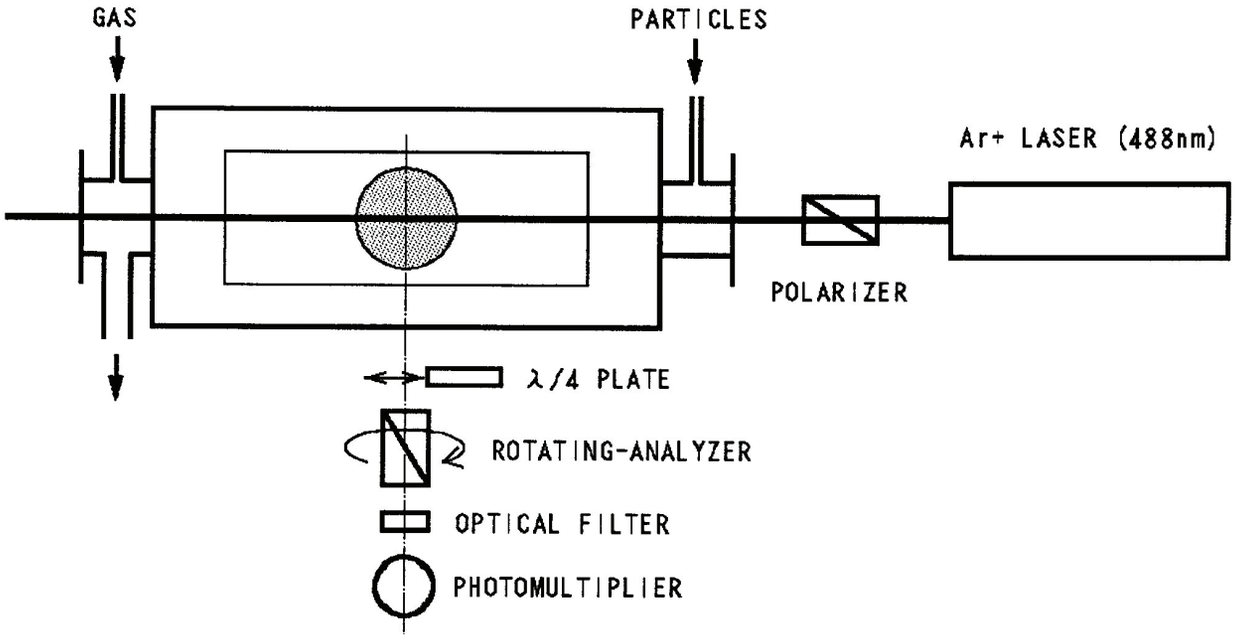

Figure 4. System configuration for Mie-scattering ellipsometry measurement in rf plasma reactor (top view).

ultra-fine particles of carbon were supplied all at once into the plasma. Then the ellipsometric measurement was started. The observation point was fixed at a position 1.2 cm below the rf electrode on the center axis, which was located in the plasma bulk.

System configuration for the measurement of Mie-scattering ellipsometry during the growth of carbon fine particles in the rf plasma reactor is shown in **Figure 4**.

3.3. *In situ* measurement by Mie-scattering ellipsometry

3.3.1. Carbon particle growth by coagulation in argon plasma

Argon gas was introduced into the chamber at a position far from the plasma region so as not to disturb or evacuate the suspended particles with its flow. After the generation of argon plasma at a pressure of 40 Pa and an rf power of 2 W, the particles of carbon soot were supplied all at once into the plasma. Then the ellipsometric measurement was started [1].

The particles were observed from the scattering light to be located at both sides of the measurement position on the laser beam line in the early period. At about 700 seconds after the injection, the light intensity gradually increased at the measurement position. The induction period depended on the experimental conditions. The evolution of the ellipsometric parameters after the initial period is shown on the Ψ-Δ coordinate plane in **Figure 5(a)**. A data point shows the average value of five measurements and data were taken every 9 seconds. During the evolution, the parameter Δ decreased gradually at first and rapidly. The evolution shows larger Δ at the beginning as compared with the calculated trajectories in **Figure 1**. It is understood from the calculation that the difference depends mainly on the employed refractive index of particles.

In order to fit the calculated trajectory to the experimental data, the simulation was carried out changing parameters; in steps of 0.1 for the real part of the refractive index, 0.05 for the

imaginary part, 1 degree for the scattering angle, and 0.1 for the geometric standard deviation along with the assumption of lognormal size distribution of polydisperse particles. The best-fit trajectory was obtained at the refractive index of 2.3–0.35*i*, the scattering angle of 91°, and the standard deviation of 1.5 as shown in **Figure 5(b)**. The smaller value of refractive index than that of evaporated carbon may be due to the inclusion of voids in the carbon particles. It can be estimated from the geometric standard deviation of 1.5 that 68% of all particles have diameters from D_m/1.5 to 1.5D_m.

From the correspondence to the best-fit trajectory, the geometric mean diameter was determined for each experimental data point. Then the particle density was evaluated with the known diameter and the measured scattered intensity. **Figure 6** gives the results and shows that the density gradually increases until the particle begins to grow and then rapidly decreases.

The bright region in the plasma formed by Mie scattering, where particles were distributed, was observed by the naked eye under the same plasma conditions. The region was initially dome-shaped. However, it became concentrated at the center axis and moved toward the rf electrode at the same time [23]. The transition may be due to the time evolution of plasma potential interacting with and interacted by negatively charged particles. The particle transfer and concentration causes coagulation, resulting in the increase of the diameter. Then, the plasma potential distribution is affected and enhances the movement. The abrupt decrease of the density at around 800 s in **Figure 6** supports this speculation.

3.3.2. Carbon particle growth by coating in methane plasma

The inlet port of methane gas was located near a pumping port so as not to disperse particles trapped in methane plasma, which was maintained under the conditions of 40 Pa gas pressure, 16 sccm gas flow rate, and 8 W rf power. Ultra-fine carbon particles were injected instantaneously into the plasma through another gas inlet port [2].

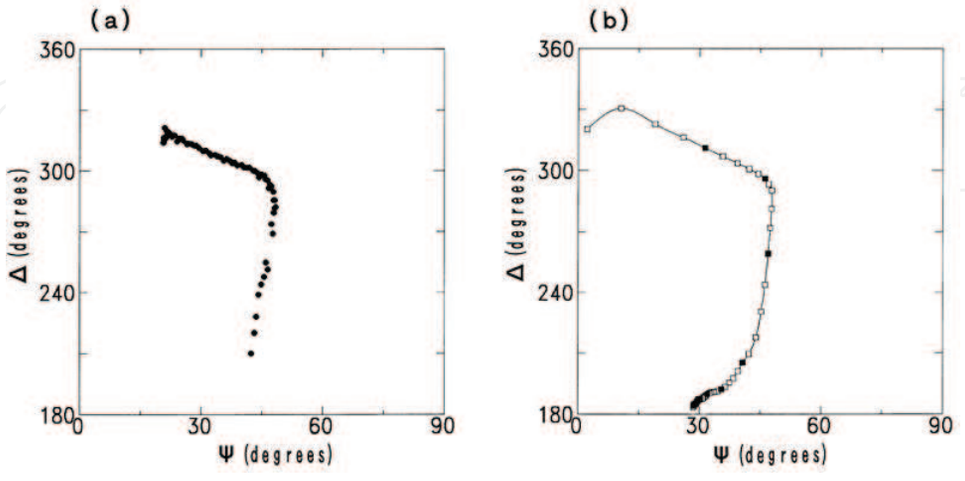

Figure 5. Experimental (a) and simulated (b) results of evolution of the ellipsometric parameters. The solid line (in (b)) shows the best-fit simulated trajectory: values used in the calculation are 2.3–0.35*i* for the refractive index and 91° for the scattering angle. The rectangles on the best-fit trajectory indicate geometric mean diameter increases every 20 nm, and the closed rectangles those every 100 nm [1].

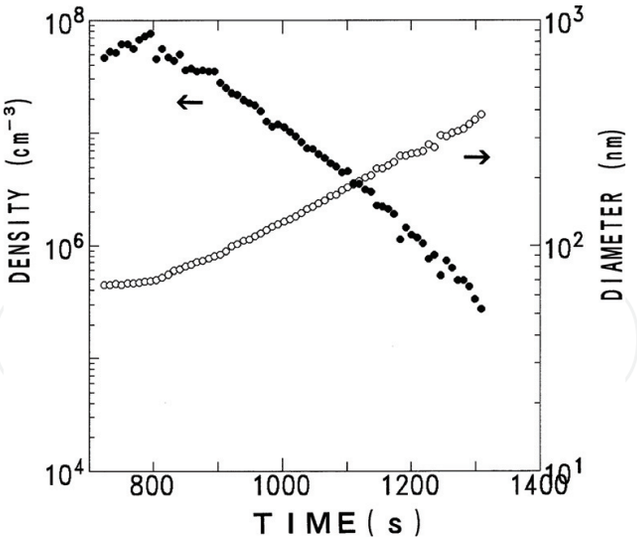

Figure 6. Evolution of density and geometric mean diameter of particles in trap at the measurement point in plasma bulk. Closed circles indicate the density and open circles the mean diameter [1].

After the injection of ultra-fine carbon particles in the plasma, the bright region of Mie scattering was observed visually. The region existed only around the sheath-plasma boundary near the rf electrode for the first 300 second, and then extended into the plasma bulk in the shape of a dome, keeping the almost same shape for about 2000 seconds.

The evolution of the ellipsometric parameters during the period is shown by points on the Ψ-Δ coordinate plane in **Figure 7**. The data were taken from 200 to 2300 seconds after the injection of ultra-fine carbon particles in the plasma. First, the parameter Ψ increased gradually with a slight change of Δ, and at $\Psi > 45°$, loops running counterclockwise were observed on the coordinate plane. Similar trajectories of the ellipsometric parameters with the same speed of

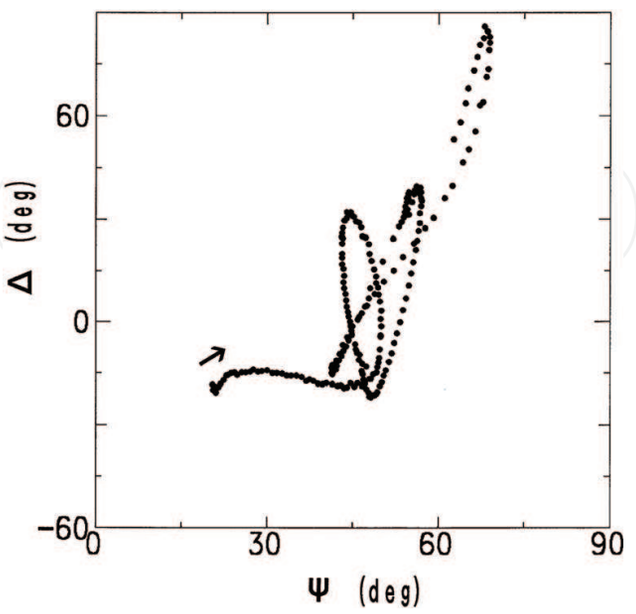

Figure 7. Experimental results of evolution of the ellipsometric parameters during carbon particle growth [2].

evolution were depicted at the other measurement positions on the center axis, except for the plasma-sheath boundaries. From the results mentioned above, it can be supposed that the particles in the plasma bulk had the same size distribution during the period.

The calculation of Mie-scattering ellipsometry of spherical polydisperse particles [1] was performed for the analysis of the experimental data. **Figure 8(a)** shows the results of the

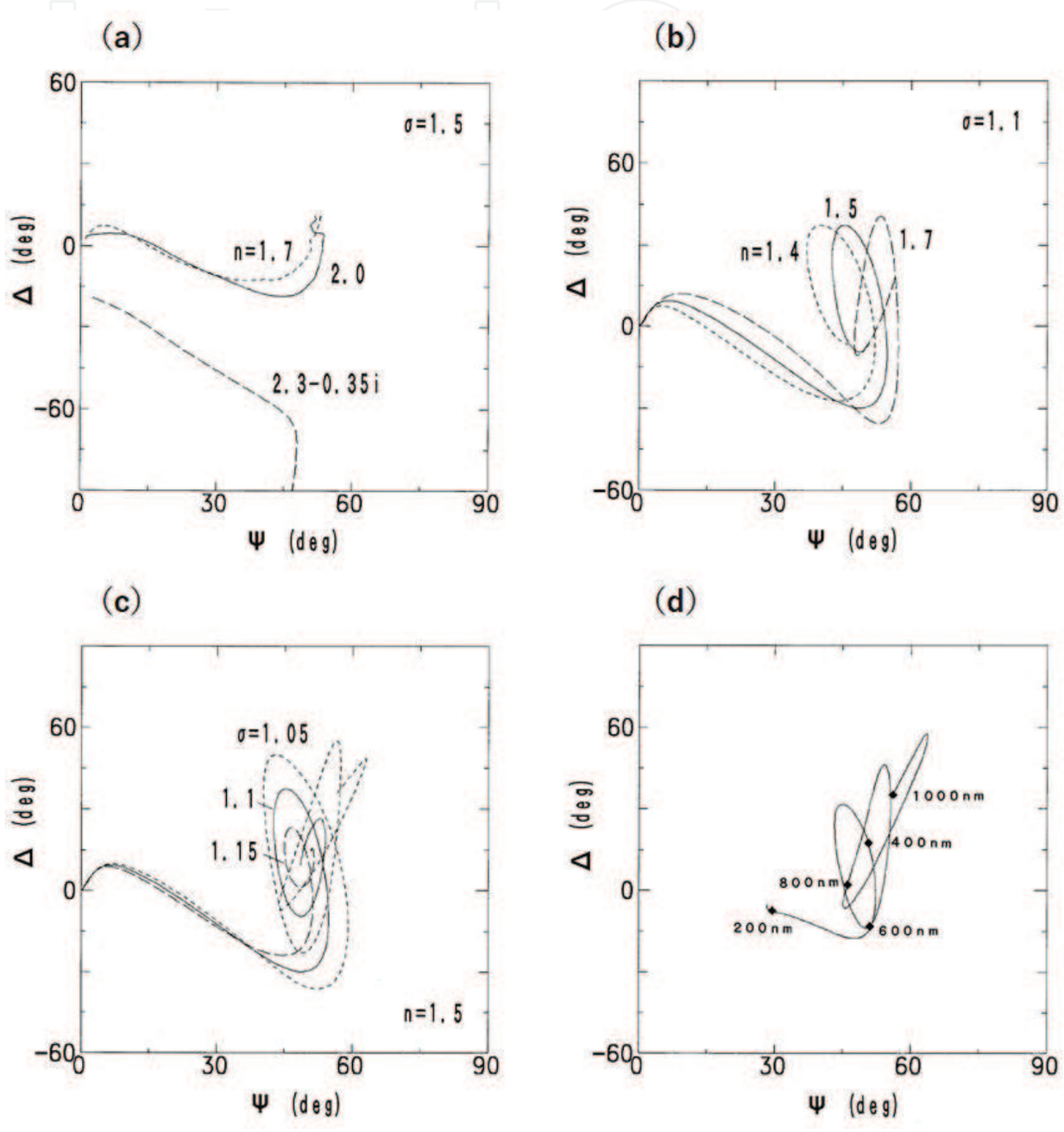

Figure 8. Evolution of the ellipsometric parameters by simulation: (a) the assumed geometric standard deviation of size distribution is 1.4, and the assumed refractive indexes are 2.3–0.35*i*, 2.0, and 1.7; (b) the assumed geometric standard deviation is 1.1, and the assumed refractive indexes are 1.7, 1.5, and 1.4; (c) the assumed geometric standard deviations are 1.15, 1.1, and 1.05, and the assumed refractive index is 1.5; (d) the translation-operated log-normal size distribution on a linear size scale is assumed with the refractive index of 1.5, and the geometric mean size and the geometric standard deviation are 50 nm and 2.0, respectively for the first lognormal distribution [2].

simulation for the growth of an ensemble of particles with a constant geometric standard deviation 1.5 for the lognormal size distribution, of which three different values of refractive index; 2.3–0.35*i*, 2.0, and 1.7, were assumed. The standard deviation and the first index are the values observed in the coagulation process of carbon particles as shown in 3.3.1. The last index is that of a hydrogenated amorphous carbon film at 488 nm [27]. As the particle diameter increases, the trajectory turned clockwise for absorbing particles, while counterclockwise for nonabsorbing particles. From the comparison of the experimental results with the calculation, it is seen that the growing particles are nonabsorbing and have the refractive index of a real number.

The calculated parameters converge to certain values while the experimental ones oscillate remarkably. Then, the calculation with a smaller geometric standard deviation of 1.1 was executed for refractive indexes of 1.7, 1.5, and 1.4 as shown in **Figure 8(b)**. It is seen that the trajectories draw loops. The inclination of the first loop of the experimental data is close to that with the index of 1.5.

Figure 8(c) shows the ellipsometric parameters in further evolution calculated in the case of a fixed refractive index of 1.5 with different geometric standard deviations of 1.15, 1.1, and 1.05. Comparing the results with the experimental trajectory, it can be seen that the standard deviation decreases with the increase of particle size, that is, the size distribution became a rather monodisperse one.

When fine particles grow by coating, size distribution function changes to that of translation-operated lognormal on a linear size scale as

$$N(D) = \frac{1}{\sqrt{2\pi}(D - D_c)\ln\sigma} e^{-\frac{\{\ln(D-D_c)-\ln D_m\}^2}{2(\ln\sigma)^2}}, \tag{8}$$

where D_c means the thickness of coated material on the seeds of ultra-fine particles of the lognormal size distribution function as Eq. (6). **Figure 8(d)** shows the result of the simulation: the geometric mean size and the geometric standard deviation for the distribution of the injected particles are 50 nm and 2.0, respectively, and the refractive index is 1.5. The simulated trajectory agrees with the experimental results better than those in **Figure 8**(a–c). The deviation of the trajectory from the experimental one at the start may be due to the difference of the refractive index between hydrogenated carbon and pure carbon.

Figure 9(a) shows the variation of the value of Δ with time for the coating growth of carbon under conditions similar to those shown above. The best-fitted trajectory by simulation was obtained for the geometric mean size and the geometric standard deviation for the distribution of the injected particles is 50 nm and 1.5, respectively, and the refractive index is 1.53. The variation of Δ value with time for the best-fitted trajectory is shown in **Figure 9(b)** [3]. Characteristics of the two curves in the peaks and dips correspond well to each other. The growing particle diameter was determined from the correspondence. The time evolution of the particle diameter so determined is plotted in **Figure 10**. It is seen that the diameter increases almost linearly for about the first 1500 seconds, then the growth rate decreases gradually. This suggests that the state of particle plasma has changed at about 1500 seconds The density of

http://dx.doi.org/10.5772/intechopen.70278

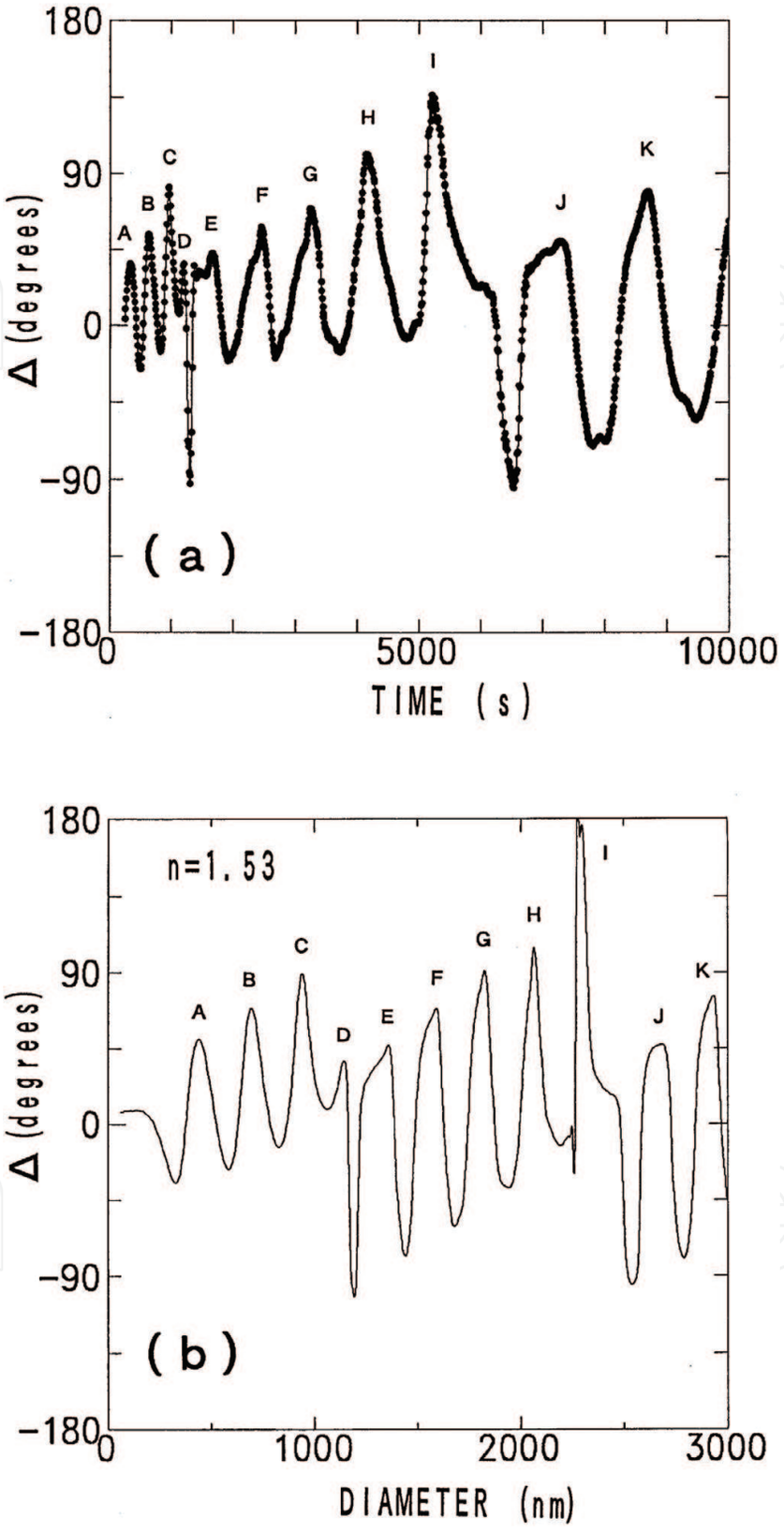

Figure 9. Experimentally obtained evolution of the ellipsometric parameter Δ with time (a), and calculated Δ as a function of the particle diameter with the refractive index 1.53 (b) [3]. The correspondence of the peaks is indicated by the same letters in both figures.

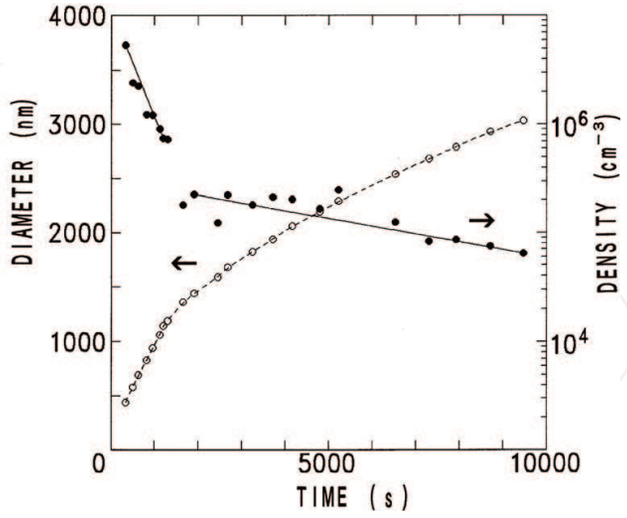

Figure 10. Evolution of particle diameter (open circles and a broken curve) and density (closed circles and solid lines) with time [3].

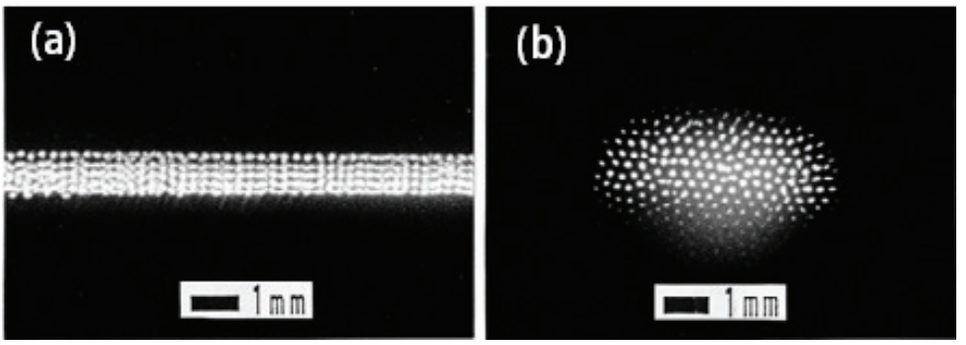

Figure 11. Photographs of a Coulomb crystal viewed from the side port (a) and the upper port (b) of the reactor [3].

particles is determined from the scattered light intensity, which is calibrated by the density evaluated from the interparticle distances in the photo of the Coulomb crystal formed in the plasma as shown in **Figure 11** [3]. It is seen in **Figure 10** that the density decrease is rapid for the first 1500 seconds, but subsequently becomes slow. It is speculated that the particles escape laterally from the plasma region through the side of the electrode gap before they are bound to one another, but they cannot escape easily after the Coulomb crystal is formed. From the consideration, it can be said that the phase transition from the state of "liquid" to that of "solid" [26] occurs at around 1500 seconds after the particle injection. At the point, the particle diameter is 1300 nm and the density is 3×10^5 cm^{-3}. The transition was also confirmed from the magnified photographs taken at times later than 1800 s, in which the particles were observed to be gradually arranged. The Wigner-Seitz radius is calculated from the density N as $[3/(4\ \pi N)]^{1/3}$ [28], and becomes about 90 μm at the phase transition.

The particles suspended in plasma were observed after the growth using a scanning electron microscope (SEM). All particles were single spheres. **Figure 12** shows a SEM micrograph for the particles suspended in plasma for 3 h. It is seen that the particles are nearly spherical and equal in size with the diameter of 3.0–3.1 μm. The spherical shape supports the former discussion on Mie-scattering ellipsometry and coating growth mechanism.

http://dx.doi.org/10.5772/intechopen.70278

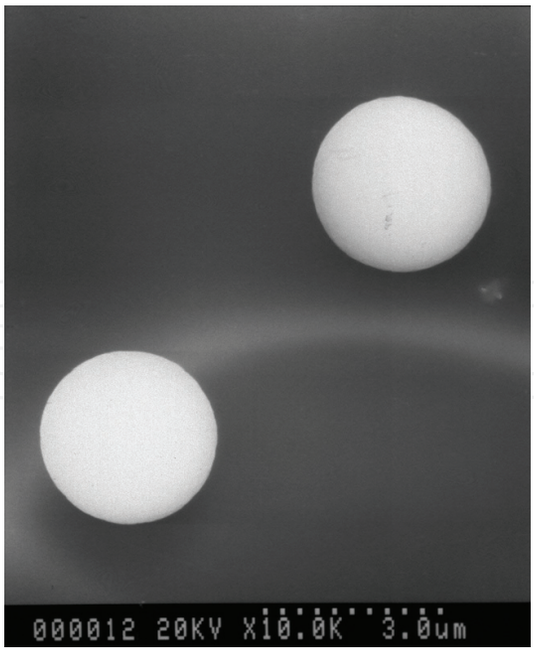

Figure 12. Typical SEM micrograph of particles suspended in plasma for 3 h.

From these results, it can be speculated about the growth of the carbon particles as follows. Hydrogenated amorphous carbon coated the ultra-fine carbon particles in methane plasma. About the smaller value of refractive index than that of a hydrogenated amorphous carbon, it can be understood that the void of 25% volume fraction was included in the coated carbon. Without the homogeneous nucleation of carbon particles in the plasma, which was confirmed by the fact that the Mie-scattered light is not observed in methane plasma without the injection of carbon ultra-fine particles under the same plasma conditions, the particles were equally coated independent of their initial size. From the spherical shape of the grown particles, it is imagined that the particles were coated isotropically. These grown particles with diameter of more than 3 μm can be suspended in methane plasma.

4. Imaging Mie-scattering ellipsometry

Imaging Mie-scattering ellipsometry, like the imaging ellipsometry for thin film analysis, enables the analysis of spatial distribution of particle size, as well as the easier confirmation of optical adjustment from a long distance. The difference between imaging Mie-scattering ellipsometer and above-mentioned Mie-scattering ellipsometer is the imaging of the distribution of fine particles using a 2D image sensor instead of a photodetector.

4.1. Experimental setup for imaging Mie-scattering ellipsometry

Ellipsometric measurement by a system with a rotating compensator has an advantage of the determination of all four Stokes parameters in one rotation. The light intensity changes by the rotation of compensator, whose azimuth is C, is expressed by sinusoidal function as [29, 30],

$$\mathcal{I}(C) = A_0 + A_2 \cos 2C + B_2 \sin 2C + A_4 \cos 4C + B_4 \sin 4C. \tag{9}$$

When the azimuth angle of the polarizer (P) and that of the analyzer (A) are 90 and ±45°, respectively, and the rotating compensator is put between the polarizer and particles, Fourier coefficients indicated in Eq. (9) are related with Ψ and Δ for particles as,

$$\Psi = \frac{1}{2} \tan^{-1} \frac{\sqrt{{B_4}^2 + \frac{1}{4}{B_2}^2}}{A_4} \quad \text{for } A_4 \geqq 0, \text{ otherwise} \bigoplus 90°, \tag{10a}$$

$$\Delta = \tan^{-1} \frac{B_2}{2B_4} \quad \text{for } B_4 < 0 (\mathrm{A} = 45°);\ B_4 \geqq 0 (\mathrm{A} = -45°), \text{ otherwise} \bigoplus 180°. \tag{10b}$$

The system for the experimental example of imaging Mie-scattering ellipsometry is shown in **Figure 13** [12]. The ellipsometer consists of polarizer and analyzer modules and a 2D image sensor. The polarizer module includes a 532 nm wavelength laser, a polarizer (P = 90°), and a rotating compensator. The analyzer module includes a wire grid polarizer (A = −45°) and a mirror. A digital video camera containing a 2D image sensor for the detection of 2D distributed

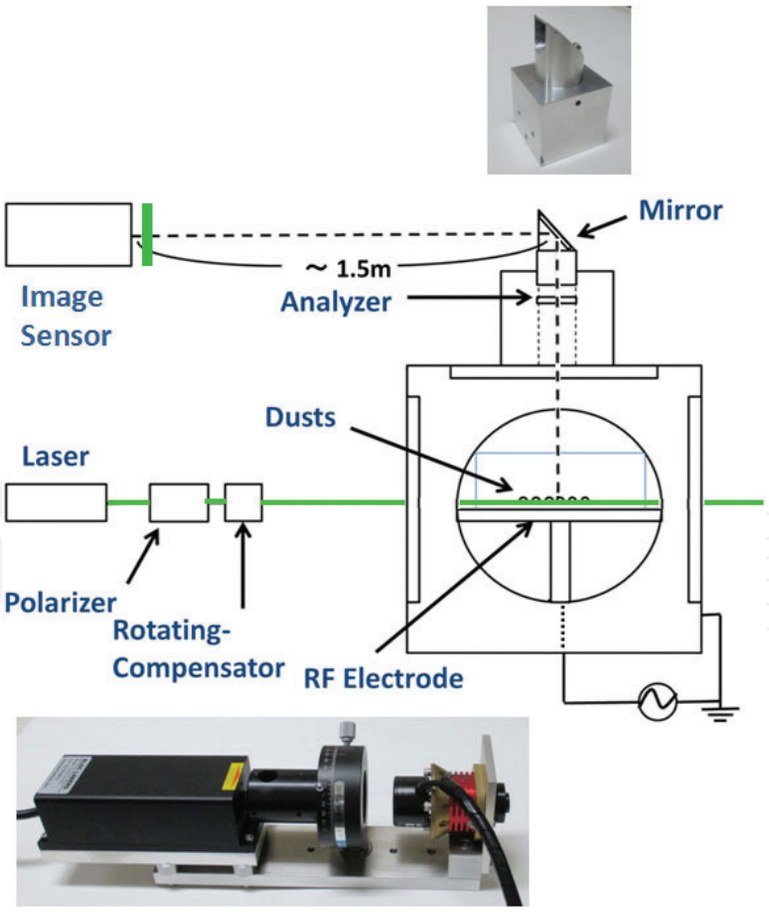

Figure 13. Schematic of ellipsometry measurement with dust plasma chamber. Inserted upper and lower photos are analyzer module and polarizer module, respectively [12].

light intensity was placed 1.5 m apart from the analyzer module. An optical band-pass filter with 1 nm FWHM at 532 nm is attached in front of the video camera. The images of distribution of fine particles by scattered light are expanded and focused using built-in functions and an extra lens. Thirty 2D images were captured every second. Although a rotating compensator is set in analyzer modules in conventional rotating-compensator ellipsometers [31, 32], it was set in the polarizer module in this case for the analyzer module able to be installed in a vacuum vessel.

The polarizer module and the digital video camera can be attached to view windows of a large plasma device in the atmosphere. The analyzer module is prepared to be fixed in a vacuum vessel [12]. It was ascertained that an image reflected by the mirror in the analyzed module could be viewed and recorded with the video camera out of the vacuum vessel of the large helical devise (LHD), a nuclear fusion experimental devise in Toki in Japan, when laser light was scattered by a small test material placed at the point of dust particle measurement.

4.2. Experiments of imaging Mie-scattering ellipsometry

In order to confirm the functional capability of the ellipsometric system, a preliminary experiment was carried out using a small dust plasma cubic chamber, 15 cm on a side [33]. Spherical divinylbenzene polymer particles of 2.27 μm in diameter with a dispersion degree of 0.1 μm were injected and suspended in argon plasma under a pressure of 50 Pa.

Light intensity data for 1600 pixels in the area covering the light scattering image were less than 75 of the maximum value of 255. Average values, i.e., total summed values of the data divided by pixel number, were calculated for images every 6° of compensator azimuth angle. The average light intensity (C_n) was obtained for each provisional azimuth angle C_n, where $C_n = 6n$. Then, Fourier analysis was performed and coefficients were obtained. After the difference between true compensator azimuth angle C and provisional one C_n was calculated through the obtained Fourier coefficients, true Fourier coefficients were calculated as

$$A_0 = 6.9009, \quad A_2 = 0, \quad B_2 = -0.9281, \quad A_4 = -1.2814, \quad B_4 = -0.6747. \tag{11}$$

Finally, ellipsometric parameters are determined by Eqs. (6a) and (6b) as

$$\Psi = 73.7^\circ, \quad \Delta = 214.5^\circ. \tag{12}$$

These values are plotted in Ψ-Δ coordinate (**Figure 14**). Meanwhile, Ψ and Δ was calculated based on the Mie scattering theory for the values of the refractive index of 1.56 (for divinylbenzene), the diameter of 2.22–2.30 μm, and the scattering angle of 90°. The calculated values are also shown in **Figure 14**. It can be stated that they agree fairly well with each other and that the measurement method is reliable. This method has the advantage of easy optical adjustment from a long distance observing the image of fine particles.

Using the same system of imaging Mie-scattering ellipsometry, the spatial size distribution of parallelly layered fine particles in argon plasma was analyzed [34]. **Figure 15** shows a video image of light scattered by spherical divinylbenzene particles of 2.74±0.09 μm in diameter

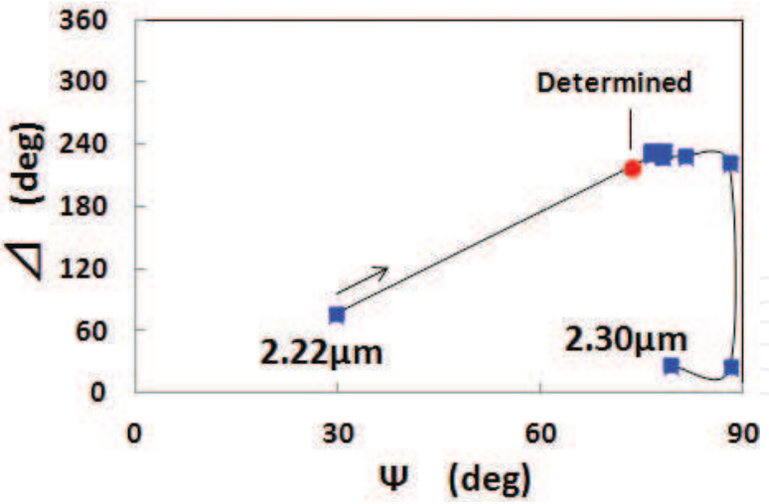

Figure 14. Ellipsometric parameters Ψ and Δ determined by measurement (circle) and calculation (squares). Calculation was carried out based on Eq. (1) and the Mie-scattering theory for the values of refractive index of 1.56, the diameter of 2.22–2.30 μm by 0.01 μm and the scattering angle of 90° [12].

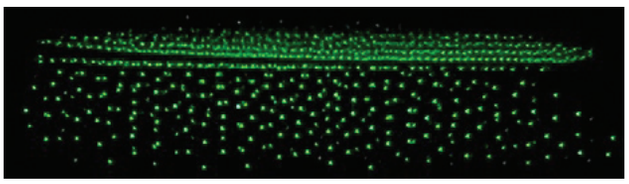

Figure 15. Video image of light scattered by spherical divinylbenzene particles of 2.74 ± 0.09 μm in diameter suspended in argon plasma at 65 Pa.

suspended in argon plasma with the pressure of 65 Pa. It is seen that the particles form vertical strings in the lower region and horizontal layers parallelly in the upper region. Fine particles more than 10 in each parallel layers were analyzed by imaging Mie-scattering ellipsometry for each area of 1320 pixels in video images. By the comparison of the determined values Ψ and Δ with calculation, the size was evaluated to be 2.70, 2.74, 2.75, and 2.77 μm for particles in upper to lower layers.

5. Conclusion

The principium of Mie-scattering ellipsometry and its analytical method were explained in detail. Then, the results of analyses by in-process Mie-scattering ellipsometry for carbon particle growth in argon plasma, as well as in methane plasma, were shown.

In argon plasma, it was suggested from the simulated trajectory best fit to the experimental data that the carbon particles included voids and the size distribution was that of polydisperse particles, such as the diameter ranging mostly from 70 to 150 nm for the mean size of 100 nm. The mean diameter and the density of particles were evaluated, and their time dependence suggests that the size increase of the particles is mostly due to coagulation.

In the case of methane plasma, the trajectory obtained by the model of translation-operated lognormal size distribution on a linear scale agreed with experimental result better than that of lognormal of a constant geometric standard deviation. It was found that ultra-fine carbon particles were coated by hydrogenated amorphous carbon during suspension in methane plasma. The particles were equally coated independent of their initial size without homogeneous nucleation in the plasma. The spherical shape of carbon particles observed in SEM image supports that the particles were coated isotropically with carbon.

An imaging Mie-scattering ellipsometry system, consisting a laser, a polarizer, a rotating compensator, an analyzer and a 2D image sensor, was developed. It was shown that the use of a 2D image sensor instead of a photodetector enables easy confirmation of optical adjustment from a long distance by the image of fine particles without any problems for measurement. The size of distributed fine particles was determined for each separated area. The developed system of imaging Mie-scattering ellipsometer has the potential for the easier confirmation of optical adjustment from a long distance, as well as for the analysis of spatial distribution of particle size.

Acknowledgements

The authors thank Mr. Masahiro Kawano and Mr. Toshihiko Arayama for experimental assistance, and Prof. Suguru Masuzaki and Prof. Kunihide Tachibana for useful discussions. This work was partly supported by the Ministry of Education, Science, Sports and Culture of Japan under Grant Number 24244094.

Author details

Yasuaki Hayashi* and Akio Sanpei

*Address all correspondence to: hayashiy@kit.ac.jp

Kyoto Institute of Technology, Kyoto, Japan

References

[1] Hayashi Y, Tachibana K. Mie-scattering ellipsometry for analysis of particle behaviors in processing plasmas. Japanese Journal of Applied Physics. 1994;**33**(3B):L476-L478. DOI: 10.1143/JJAP.33.L476

[2] Hayashi Y, Tachibana K. Analysis of spherical carbon particle growth in methane plasma by Mie-scattering ellipsometry. Japanese Journal of Applied Physics. 1994;**33**(7B):4208-4211. DOI: 10.1143/JJAP.33.4208

[3] Hayashi Y, Tachibana K. Observation of Coulomb-Crystal formation from growing particles grown in a methane plasma. Japanese Journal of Applied Physics. 1994;**33**(6A):L804-L806. DOI: 10.1143/JJAP.33.L804

[4] Chu JH, Lin I. Direct observation of Coulomb crystals and liquids in strongly coupled rf dusty plasmas. Physical Review Letters. 1994;**72**(25):4009-4012. DOI: 10.1103/PhysRevLett.72.4009

[5] Thomas H, Morfill GE, Demmel V, Goree J, Feuerbach B, Möhlmann D. Plasma crystal: Coulomb crystallization in a dusty plasma. Physical Review Letters. 1994;**73**(5):652-655. DOI: 10.1103/PhysRevLett.73.652

[6] Tachibana K, Hayashi Y. Analysis of the Coulomb-solidification process in particle plasma. Australian Journal of Physics. 1995;**48**:469-477. DOI: 10.1071/PH950469

[7] Hayashi Y, Tachibana K. Coulomb crystal formation from growing particles in a plasma and the analysis. Journal of Vacuum Science and Technology. 1996;**14**(2):506-510. DOI: 10.1116/1.580116

[8] Hong SH, Winter J. Size dependence of optical properties and internal structure of plasma grown carbonaceous nanoparticles studies by in situ Rayleigh-Mie scattering ellipsometry. Journal of Applied Physics. 2006;**100**:064303. DOI: 10.1063/1.2338132

[9] Groth S, Greiner F, Tadsen B, Piel A. Kinetic Mie ellipsometry to determine the time-resolved particle growth in nanodusty plasmas. Journal of Physics D: Applied Physics. 2015;**48**:465203. DOI: 10.1088/0022-3727/48/46/465203

[10] Shiratani M, Kawasaki H, Fukuzawa T, Yoshioka T, Ueda Y, Singh S, Watanabe Y. Simultaneous in situ measurements of properties of particulates in rfsilane plasmas using a polarization-sensitive laser-light-scattering method. Journal of Applied Physics. 1996;**79**(1):104-109. DOI: 10.1063/1.360916

[11] Greiner F, Carstensen J, Kohler N, Pilch I, Ketelsen H, Knist S, Piel A. Imaging Mie-ellipsometry: Dynamics of nanodust clouds in an argon-acetylene plasma. Plasma Sources, Science and Technology. 2012;**21**(6):065005. DOI: 10.1088/0963-0252/21/6/065005

[12] Hayashi Y, Kawano M, Sanpei A, Masuzaki S. Mie-scattering ellipsometry system for analysis of dust formation process in large plasma device. IEEE Transactions on Plasma Science. 2016;**44**(6):1032-1035. DOI: 10.1109/TPS.2016.2542349

[13] Kerker M. The use of white light in determining particle radius by the polarization ratio of the scattered light. Journal of Colloidal Science. 1950;**5**:165-167

[14] Azzam RMA, Bashara NM. Ellipsometry and Polarized Light. Amsterdam: North Holland; 1987. p. 539

[15] Theeten JB, Hottier F, Hallais J. Ellipsometric assessment of (Ga, Al) As/GaAs epitaxial layers during their growth in an organometallic VPE system. Journal of Crystal Growth. 1979;**46**(2):245-252. DOI: 10.1016/0022-0248(79)90064-2

[16] Theeten JB. Real-time and spectroscopic ellipsometry of film growth: Application to multilayer systems in plasma and CVD processing of semiconductors. Surface Science. 1980;**96**(1-3):275-293. DOI: 10.1016/0039-6028(80)90307-6

[17] Hayashi Y, Itoh A. Ellipsometric monitor for film thickness control in plasma processes. In: Proceedings of International Ion Engineering Congress, ISIAT'83 & IPAT'83; Kyoto, Japan. 1983. pp. 1469-1474

[18] Collins RW, Pawlowski A. The nucleation and growth of glow-discharge hydrogenated amorphous silicon. Journal of Applied Physics. 1986;**59**(4):1160-1166. DOI: 10.1063/1.336553

[19] Antoine AM, Drevillon B, Roca i Cabarrocas P. In situ investigation of the growth of rf glow-discharge deposited amorphous germanium and silicon films. Journal of Applied Physics. 1987;**61**(7):2501-2508. DOI: 10.1063/1.337924

[20] Hayashi Y, Drawl W, Collins RW, Messier R. In-process ellipsometric monitoring of diamond film growth by microwave plasma enhanced chemical vapor deposition. Applied Physics Letters. 1992;**60**(23):2868-2870. DOI: 10.1063/1.106827

[21] Hayashi Y, Drawl W, Messier R. Temperature dependence of nucleation density of chemical vapor deposition diamond. Japanese Journal of Applied Physics. 1992;**31**(2B):L193-L196. DOI: 10.1143/JJAP.31.L193

[22] van de Hulst HC. Light Scattering by Small Particles. New York: Dover; 1981. p. 470

[23] Tachibana K, Hayashi Y, Okuno T, Tatsuta T. Spectroscopic and probe measurements of structures in a parallel-plates RF discharge with particles. Plasma Sources Science and Technology. 1994;**3**(3):314-319. DOI: 10.1088/0963-0252/3/3/012

[24] Deirmendjian D. Electromagnetic Scattering on Spherical Polydispersions. New York: American Elsevier; 1969. p. 290

[25] Yoshida T, Okuyama K, Kousaka Y, Kida Y. Change in particle size distributions of polydisperse aerosols undergoing Brownian coagulation. Journal of Chemical Engineering of Japan. 1975;**8**(4):317-322. DOI: 10.1252/jcej.8.317

[26] Hayashi Y. Thin film monitoring with ellipsometry in in-line processing equipment. Japanese Journal of Applied Physics. 1990;**29**(11):2514-2518. DOI: 10.1143/JJAP.29.2514

[27] Ikezi H. Coulomb solid of small particles in plasmas. The Physics of Fluids. 1986;**29**:1764-1766. DOI: 10.1063/1.865653

[28] Ichimaru S. Strongly coupled plasmas: High-density classical plasmas and degenerate electron liquids. Reviews of Modern Physics. 1982;**54**(4):1017-1059. DOI: 10.1103/RevModPhys.54.1017

[29] Hauge PS, Dill FH. A rotating-compensator Fourier ellipsometer. Optics Communications. 1975;**14**(4):431-437. DOI: 10.1016/0030-4018(75)90012-7

[30] Hauge PS. Generalized rotating-compensator ellipsometry. Surface Science. 1976;**56**:148-160. DOI: 10.1016/0039-6028(76)90442-8

[31] Lee J, Rovira PI, An I, Collins RW. Rotating-compensator multichannel ellipsometry: Applications for real time Stokes vector spectroscopy of thin film growth. Review of Scientific Instruments. 1998;**69**(4):1800-1810. DOI: 10.1063/1.1148844

[32] Weiß R, Hong S-H, Ränsch J, Winter J. Rayleigh. Mie scattering ellipsometry as an in situ diagnostic for the production of 'smart nanoparticles'. Physica Status Solidi A. 2008;**205**(4): 802-805. DOI: 10.1002/pssa.200777803

[33] Hayashi Y, Mizobata Y, Takahashi K. Experiments of fine-particle plasma using planar magnetron plasma system. International Journal of Microgravity Science and Application. 2011;**28**(2):S23-S26

[34] Hayashi Y, Sanpei A, Mieno T, Masuzaki S. Analysis of spatial distribution of fine particles in plasma by imaging Mie-Scattering ellipsometry. In: 8th International Conference on the Physics of Dusty Plasmas; 20-25 May 2017; Prague, Czech Republic